Three-dimensional numerical simulations of free convection in a layered porous enclosure

Fernando J. Guerrero-Martínez*, Paul L. Younger, Nader Karimi, Sotirios Kyriakis

School of Engineering, University of Glasgow, Glasgow G12 8QQ, Scotland, UK.

Abstract

Three-dimensional numerical simulations are carried out for the study of free convection in a layered porous enclosure heated from below and cooled from the top. The system is defined as a cubic porous enclosure comprising three layers, of which the external ones share constant physical properties and the internal layer is allowed to vary in both permeability and thermal conductivity. The model is based on Darcy's law and the Boussinesq approximation. A parametric study to evaluate the sensitivity of the Nusselt number to a decrease in the permeability of the internal layer shows that strong permeability contrasts are required to observe an appreciable drop in the Nusselt number. If additionally the thickness of the internal layer is increased, a further decrease in the Nusselt number is observed as long as the convective modes remain the same, if the convective modes change the Nusselt number may increase. Decreasing the thermal conductivity of the middle layer causes first an increment in the Nusselt number and then a drop. On the other hand, the Nusselt number decreases in an approximately linear trend when the thermal conductivity of the layer is increased.

Keywords: 3D numerical modeling, free convection, porous medium, Boussinesq approximation.

*Corresponding author. Tel.: +44 (0) 141 330 5042
Email address: `f.guerrero-martinez.1@research.gla.ac.uk` (Fernando J. Guerrero-Martínez)

June 17, 2016

Nomenclature

β	Thermal expansion coefficient
$\boldsymbol{\psi}$	Vector potential
$\mathbf{u}$	Dimensionless velocity
η	Thermal diffusivity
μ	Viscosity
ρ_0	Density of reference
θ	Dimensionless temperature
g	Gravitational constant
k	Permeability
L	Characteristic length
Nu	Nusselt number
P	Dimensionless pressure
Ra	Darcy-Rayleigh number
Ra_c	Critical Rayleigh number
T	Dimensional temperature
t	Dimensionless time
x, y, z	Dimensionless coordinates

1. Introduction

The problem of free convection in layered porous media has been of great interest in research due to the its presence in both nature and engineering processes. Geothermal reservoir and ground water modeling are examples of the application fields of this topic. Thermal gradients in fractured-porous media can drive convective flow [1], and create thermal anomalies of interest in geothermal applications [2, 3, 4]. The study of convective heat transfer in layered porous media is particularly important, since the presence of high (or low) permeability strata is a geological feature commonly found in hydrothermal systems. In this paper we present 3D steady-state numerical simulations of free convection in a three-layer porous enclosure.

Early work on the onset of convection in layered porous media is that by McKibbin and O'Sullivan [5, 6]. They studied two and three-layer systems considering constant thermal conductivity in a two-dimensional cell. They defined a Rayleigh number referred to the physical properties of the bottom layer and the total thickness and temperature drop of the enclosure. From linear stability analysis they calculated critical values (Ra_c) as a function of the permeability ratio. They found that considerably high permeability ratios between layers (~ 20) are required to observe convective modes different from those for a homogeneous porous medium, these convective modes are characterized by some degree of confinement of convection in the high-permeability layers. Richard and Gounot [7] studied the onset of convection in a layered porous medium considering both anisotropic and isotropic layers as regards the permeability and thermal conductivity. As a particular case study, they calculated numerically Ra_c for the onset of convection for a two-layer porous medium with isotropic layers and showed that the stability of the system increases when the permeability of the upper layer is decreased, their definition of Ra was based on a weighted average of permeability and thermal conductivity on the thickness of the layers. The magnitude of this increase was in turn dependent on the relative thickness of the layers. In a similar two-layer model Rosenberg and Spera [8] reported an asymptotical increase in the Nusselt number as the permeability ratio of the top to the bottom layers was increased, they observed confinement of convection for a permeability ratio of the top to the bottom layers of 10 and $Ra = 35$ which was defined with respect to the bottom layer of the system. Mckibbin and Tyvand [9] investigated the conditions under which thermal convection in a layered porous medium can be comparable to that for an anisotropic porous medium. They pointed out that a multilayer system can be modeled by an analog anisotropic system when there is no confinement of convection in the layered system.

The problem of porous layers separated by conductive impermeable interfaces has also been investigated. Jang and Tsai [10] studied the onset of convection in a two-layer system separated by a conductive interface. They defined an overall Rayleigh number considering the total thickness of the arrangement of layers and found that the presence of the impermeable layer increases considerably the stability of the system, being the most stable those cases with the impermeable layer located in the middle of porous cell. More recently Rees and Genç [11] studied multilayer systems separated impermeable interfaces of negligible thickness and observed that Ra_c, defined locally in each layer, tends asymptotically to 12 as the number of sublayers is increased. Patil and Rees [12] extended the study to consider finite thickness of the conductive interfaces so that the conductivity had an impact on the behaviour of the system. They reported that Ra_c and the associated wave number decreased when the thermal conductivity of the solid interfaces was decreased. Hewitt et al. [13] determined statistical steady-state convection at high Ra in a 2D periodic porous enclosure. Their model consists of a thin low permeability layer sandwiched by two high permeability layers. Regarding the convective modes, they found that for a given Ra and permeability ratio, an increase in the thickness leads to an ordered array of cells with stratification of the flow. On the other hand, they noted that the Nusselt number as a function of thickness of the low permeability layer experiences first a small increase for small thickness and then it decreases for larger thickness.

Although the scope of this work is layered porous media, it is important to mention the work by Nield and Kustnetzov [14, 15] who investigated the effect of weak and moderate vertical and horizontal heterogeneities. They defined a Rayleigh number based on the mean properties of the porous enclosure and found that these heterogeneities lead to a decrease in Ra_c for all combinations of horizontal and vertical heterogeneities and all combinations of permeability and conductivity heterogeneities. Vertical heterogeneity proved to have greater influence than horizontal heterogeneity, presumably due to the influence of gravity. Likewise, Capone [16] found that an increase in the permeability in the upward direction is destabilizing whereas an increase in the downward direction is stabilizing. Nield and Kuznetsov [17] reported that horizontal variations in both permeability and thermal diffusivity lead to slight destabilization in comparison with vertical variations.

The aim of this study is to obtain 3D steady-state numerical solutions of free convection in a three-layer porous enclosure. The steady-state solutions are obtained from the simulation of the transient problem applying a convergence criterion. A parametric study is carried out to evaluate the Nusselt number as a function of the permeability, thermal conductivity, and thickness of the internal layer of the system.

2. Problem formulation

The porous enclosure consists of a three-layer system, of which the external layers have the same and constant physical properties and the internal may differ as regards the permeability and thermal conductivity (Figure 1). It is assumed that the porous medium is isotropic within each layer. Fluid flow is governed by Darcy's law and buoyancy effects are described by the Boussinesq approximation. Local thermal equilibrium and negligible viscous heat generation are additional assumptions in this problem. From these considerations the momentum equation can be written in the following form (we use bar notation to denote dimensional variables and operators):

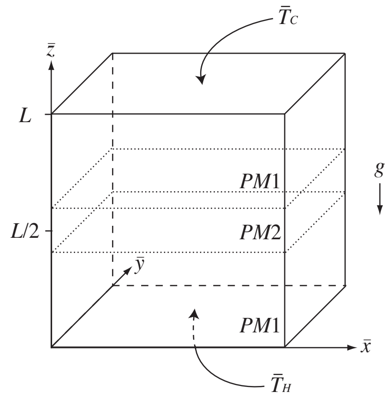

Figure 1: Schematic model of a layered porous enclosure heated from below and cooled from the top with adiabatic lateral boundaries. The external layers ($PM1$) have constant properties, whereas the properties of $PM2$ are allowed to vary.

$$\bar{\mathbf{u}} = -\frac{k(z)}{\mu}\left(\bar{\nabla}\bar{P} - \rho_0 g \beta(\bar{T} - \bar{T}_0)\hat{\mathbf{k}}\right) \tag{1}$$

Where the permeability is defined as $k(z) = f(z)k_1$, with k_1 the permeability referred to that for the top and bottom layers, and $f(z)$ is a dimensionless smooth function, which in this case will be defined as a hyperbolic tangent function to represent layers. The energy equation is as follows

$$\frac{\partial \bar{T}}{\partial \bar{t}} + \bar{\mathbf{u}} \cdot \bar{\nabla}\bar{T} = \bar{\nabla} \cdot (\eta(z)\bar{\nabla}\bar{T}) \tag{2}$$

Likewise, the thermal diffusivity is defined as $\eta(z) = g(z)\eta_1$, with η_1 referred to $PM1$ and $g(z)$ a smooth function to represent layers. The condition of incompressibility of the fluid is also invoked:

$$\bar{\nabla} \cdot \bar{\mathbf{u}} = 0 \tag{3}$$

Dimensionless variables are defined as follows:

$$x = \frac{\bar{x}}{L} \qquad y = \frac{\bar{y}}{L} \qquad z = \frac{\bar{z}}{L} \qquad P = \frac{k_1}{\mu\eta_1}\bar{P}$$

$$\mathbf{u} = \frac{L}{\eta_1}(\bar{u}, \bar{v}, \bar{w}) \quad \theta = \frac{\bar{T} - \bar{T}_0}{\bar{T}_0 - \bar{T}_c} \quad t = \frac{\bar{t}\eta_1}{L^2}$$

$$Ra = \frac{L k_1 g \beta \rho_0}{\eta_1 \mu}(\bar{T}_0 - \bar{T}_c)$$

Where Ra is the Darcy-Rayleigh number and L the characteristic length. The dimensionless problem is then as follows, momentum equation:

$$\frac{1}{f(z)}\mathbf{u} + \nabla P = Ra\theta\hat{\mathbf{k}} \tag{4}$$

The dimensionless energy equation is as follows:

$$\frac{\partial \theta}{\partial t} + \mathbf{u} \cdot \nabla \theta = \nabla \cdot (g(z)\nabla\theta) \tag{5}$$

A global Nusselt number is defined to quantify the heat transfer through the upper surface $z = 1$:

$$Nu = \int \left|\frac{\partial \theta}{\partial z}\right|_{z=1} dA \tag{6}$$

2.1. Boundary conditions and initial conditions

As initial condition both dimensionless temperature and velocity are set to zero. The lateral walls of the enclosure are adiabatic and the bottom and top boundaries have specified temperatures, so that the boundary conditions for the energy equation can be written as

$$\frac{\partial \theta}{\partial x} = 0, \quad \text{for} \quad x = 0 \quad \text{and} \quad x = 1$$
$$\frac{\partial \theta}{\partial y} = 0, \quad \text{for} \quad y = 0 \quad \text{and} \quad y = 1$$

$$\theta = 1, \quad \text{for} \quad z = 0 \quad \text{and} \quad \theta = 0, \quad \text{for} \quad z = 1 \quad \text{for} \quad t > 0$$

Regarding the momentum equation impermeable boundary conditions are assumed. The implementation of these boundary conditions is described in the following section.

3. Numerical solution

The numerical implementation was carried out following the vector potential approach. Pressure is eliminated from the momentum equation (Eq. 4) by taking the curl:

$$\nabla \times \left(\frac{1}{f(z)} \mathbf{u} \right) = Ra \nabla \times \theta \hat{\mathbf{k}} \tag{7}$$

This equation is then written in terms of a vector potential $\boldsymbol{\psi}$, such that $\mathbf{u} = \nabla \times \boldsymbol{\psi}$ and $\nabla \cdot \boldsymbol{\psi} = 0$. The components of the momentum equation turn out:

$$\begin{cases} \nabla^2 \psi_1 = -Ra \frac{\partial \theta}{\partial y} - \frac{f'(z)}{f^2(z)} v \\ \nabla^2 \psi_2 = Ra \frac{\partial \theta}{\partial x} + \frac{f'(z)}{f^2(z)} u \\ \nabla^2 \psi_3 = 0. \end{cases} \tag{8}$$

The corresponding boundary conditions are:

$$\frac{\partial \psi_1}{\partial x} = \psi_2 = \psi_3 = 0, \quad \text{for} \quad x = 0 \quad \text{and} \quad x = 1$$

$$\frac{\partial \psi_2}{\partial y} = \psi_1 = \psi_3 = 0, \quad \text{for} \quad y = 0 \quad \text{and} \quad y = 1$$

$$\frac{\partial \psi_3}{\partial z} = \psi_1 = \psi_2 = 0, \quad \text{for} \quad z = 0 \quad \text{and} \quad z = 1$$

The system can be further simplified noticing that $\psi_3 = 0$. The problem given by Equations 5 and 8 with the corresponding boundary conditions was discretized following the Finite Volume numerical method [18]. The numerical algorithm was based on a fixed point iteration and was implemented in Fortran with parallel computing in OpenMP (more details of the numerical model can be founded in our previous work [19]). Steady state solutions were determined from long simulation times using a convergence criterion based on the evaluation of the change in the temperature field during the last 2.2×10^3 successive iterations which proved to be long enough, convergence was defined when the average maximum change in the matrix of temperature was less than 5×10^{-7}. A time step $\Delta t = 2 \times 10^{-5}$ and a uniform mesh size $\Delta x = \Delta y = \Delta z = 100^{-1}$ were employed in all the simulations.

4. Numerical results and discussion

4.1. Validation

The validation of our model for the homogeneous case was presented in a previous work [19]. A validation for the layered model is presented here considering the results reported by McKibbin and O'Sullivan [5]. For a three-layer porous enclosure with a thickness of the middle layer $h = 0.2$ the authors reported a $Ra_c \simeq 300$ for a wave number $n = 4$ and a permeability contrast $k_2/k_1 = 0.01$. For these conditions a convective mode composed by four convective rolls confined in the top and bottom layers was reported. A simulation was carried out with our 3D model for the same thickness, Rayleigh number and permeability ratio. The result was consistent with that reported in the referred work. The steady-state temperature and velocity fields are shown in Figure 2 and the stream lines of a 2D section in Figure 3.

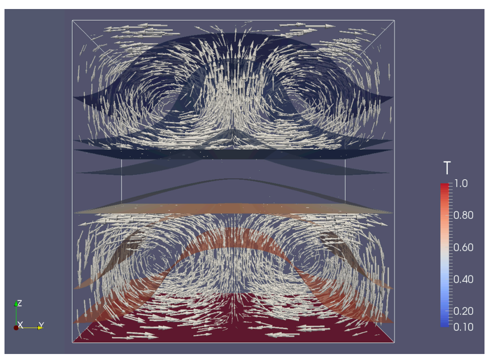

Figure 2: Steady-state temperature and velocity fields for $k_2/k_1 = 0.01$, $h = 0.2$, and $Ra = 300$. The corresponding Nusselt number for this result was $Nu = 1.43$.

4.2. Nu vs permeability ratio and internal layer thickness

Let us discuss first the effect of the permeability ratio and internal layer thickness on the Nusselt number. All the simulations were carried out consider-

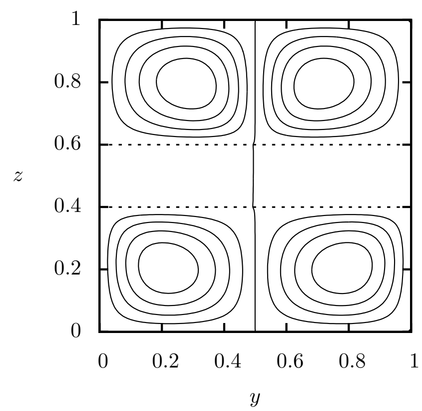

Figure 3: Streamlines calculated at the section $x = 0.5$ of Figure 2.

ing a constant $Ra = 200$ and three thicknesses were evaluated, $h = 0.1$, $h = 0.15$ and $h = 0.2$. Jang and Tsai [10] reported critical Rayleigh numbers between 141 and 213 in this range of thicknesses and considering impermeable internal layer, so that $Ra = 200$ was considered to be large enough to observe convection in the cases analyzed here. Figure 4 shows the steady-state Nusselt number for the three thicknesses analyzed. It can be observed that for relatively low permeability ratio there is a very small change in the Nusselt number, significant differences are observed only around $k_2/k_1 = 0.6$. Furthermore, there is first a slight increase in Nu when the permeability ratio is decreased from 1. Secondly, for high permeability contrast Nu is not necessarily inversely proportional to h as it can be seen at $k_2/k_1 = 0.2$, a similar behaviour was reported by Hewitt et al. [13] in the context of thin layers and high Ra. In this study however, the reason for this behaviour is that the convective modes attained in each thickness is not necessarily the same.

All the convective modes observed in these simulations were characterized by 2D cells. Figure 5 shows streamlines calculated at different cross sections perpendicular to the axis of the convective cells. For $k_2/k_1 = 0.01$ it is observed confinement of convection for $h = 0.1$ and $h = 0.15$. When the thickness is increased to $h = 0.2$ however, the system becomes conductive, as shown by

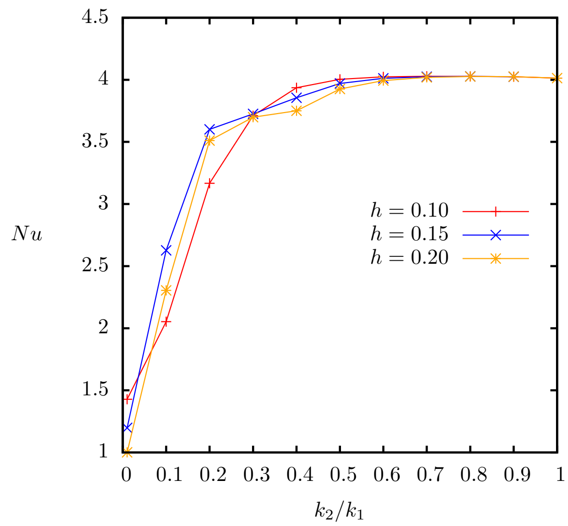

Figure 4: Nusselt number vs permeability ratio for three different internal layer thicknesses.

the Nusselt number $Nu = 1.0$ (Figure 4). $k_2/k_1 = 0.1$ shows that $h = 0.1$ remains essentially as confined convection, whereas $h = 0.15$ and $h = 0.2$ present convection throughout the entire enclosure (Figure 6), this convective mode enhances the heat transfer as shown by a larger Nusselt number of these cases in comparison with $h = 0.1$. The same is true for $k_2/k_1 = 0.2$, although in this case there is no confinement, $h = 0.1$ presents a four-cell convective mode that reduces the convective heat transfer in the system in comparison with $h = 0.15$ and $h = 0.2$, both characterized by two cells partially confined in the top and bottom layers. For the case $k_2/k_1 = 0.3$ the Nusselt number was almost the same (Figure 4), despite the convective mode, Figure 7 shows the convective modes for $h = 0.1$ and $h = 0.2$. For this permeability ratio, the orientation of the convective cells was not coincident as shown in the case $h = 0.15$, which convective cell was oriented in the y-axis direction. In summary, a strong permeability contrast is required ($k_2/k_1 < 0.5$) to notice a considerable impact on the Nusselt number of the enclosure. Likewise, both thickness and convective mode are important to determine how the Nusselt number is affected.

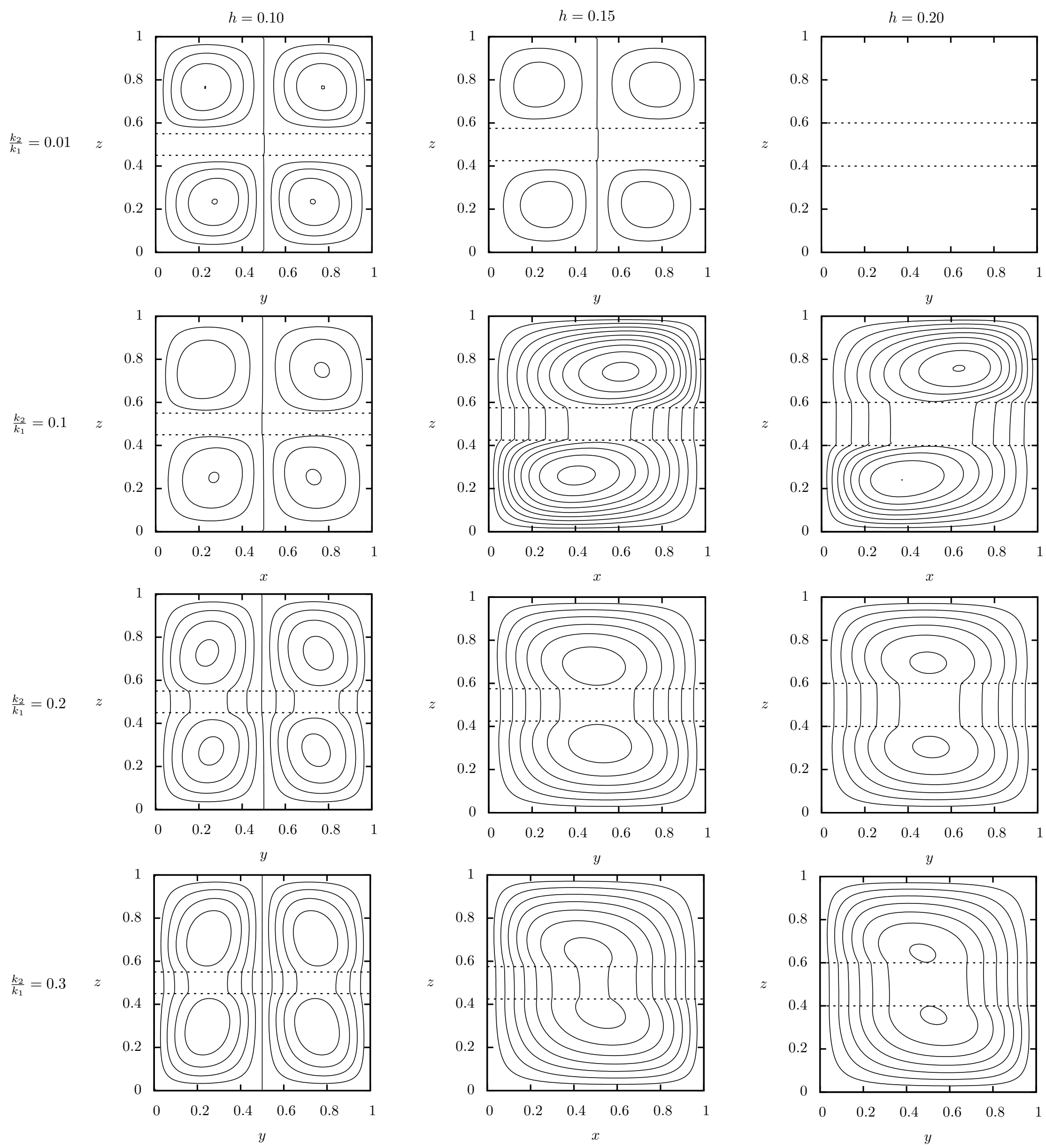

Figure 5: Stream lines at the cross section $x = 0.5$ and $y = 0.5$ for high permeability contrast. The corresponding Nusselt numbers are shown in Figure 4.

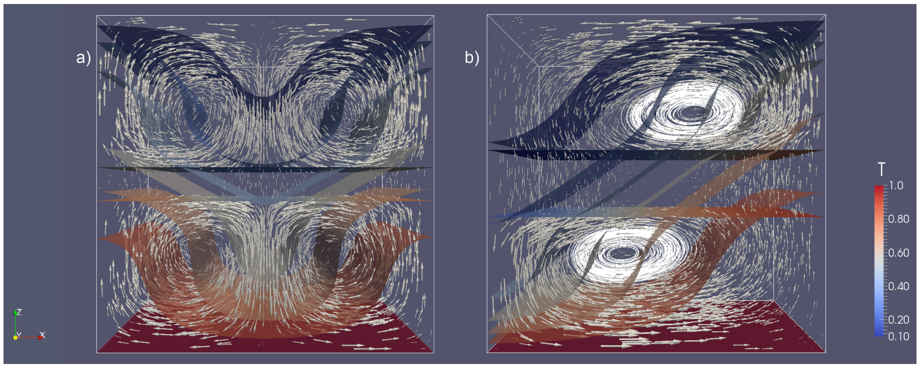

Figure 6: Steady-state solutions for $k_2/k_1 = 0.1$ and a) $h = 0.1$ and b) $h = 0.2$

4.3. Nu vs conductivity ratio

The evaluation of the conductivity ratio was carried out considering a constant thickness $h = 0.1$ and $Ra = 200$ for two permeability ratios. No attempt is made here to follow a model for the relation between thermal conductivity and permeability, a presentation of such models can be referred to Bear [20]. Steady state Nusselt numbers of the studied cases are presented in Figure 8.

4.3.1. Internal layer with low thermal conductivity ($\eta_2/\eta_1 < 1$)

Let us discuss first the case $\eta_2/\eta_1 < 1$, in which the internal layer acts as a low thermal conductivity layer. In this case, in both permeability ratios, a slight

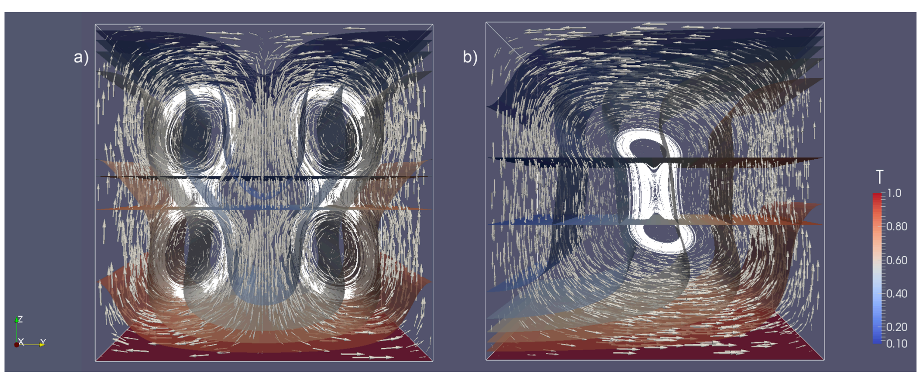

Figure 7: Steady state solutions for $k_2/k_1 = 0.3$ and a) $h = 0.1$ and b) $h = 0.2$

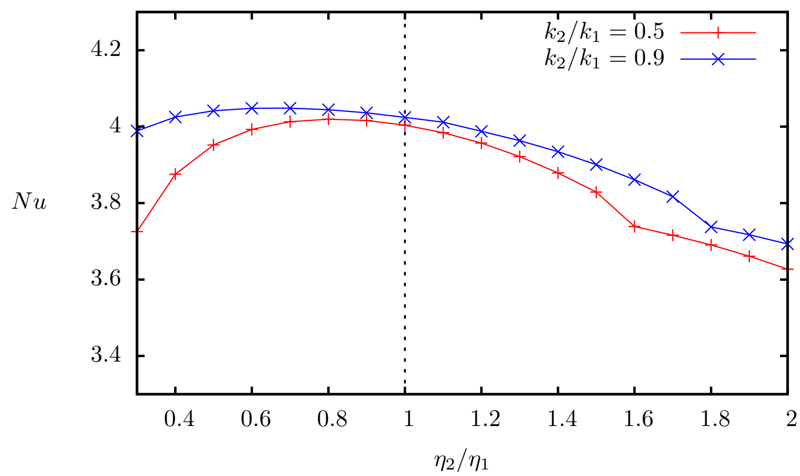

Figure 8: Nusselt number vs conductivity ratio for a constant thickness $h = 0.1$ and $Ra = 200$.

increase in Nu was observed first as the thermal conductivity of the layer was decreased and subsequently Nu decreases. This behaviour can be understood as a destabilizing effect of decreasing the thermal conductivity, a further reduction in η_2 leads to a drop in Nu as the isolating effect of the layer becomes more important. Regarding the permeability ratio $k_2/k_1 = 0.5$, a high sensitivity to the thermal diffusivity ratio was observed for $\eta_2/\eta_1 < 0.5$, for these values the layer behaves more effectively as a barrier for the heat flux. The convective

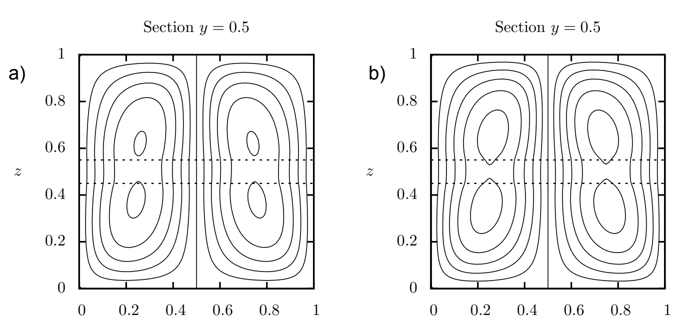

Figure 9: Stream lines for $k_2/k_1 = 0.5$ and a) $\eta_2/\eta_1 = 0.2$, b) $\eta_2/\eta_1 = 1.0$.

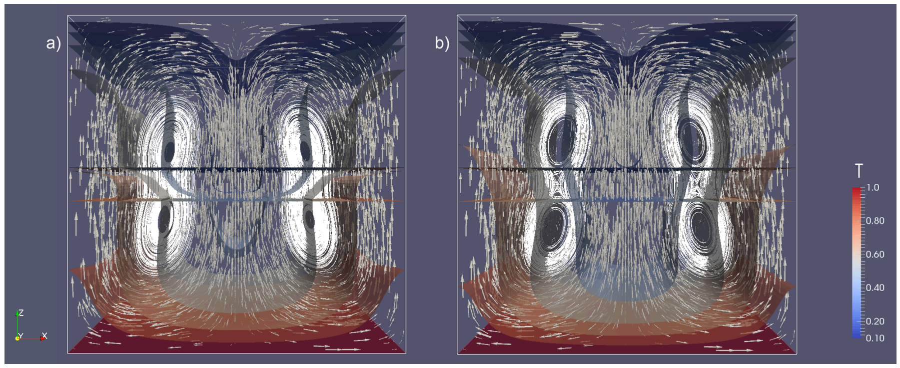

Figure 10: Steady-state solutions for $k_2/k_1 = 0.5$ and a) $\eta_2/\eta_1 = 0.2$, b) $\eta_2/\eta_1 = 1.0$.

modes for this permeability ratio were characterized by two main convective cells with secondary internal cells separated by the middle layer. Stream lines are shown in Figure 9 and the corresponding temperature and velocity fields in Figure 10.

On the contrary, for a weak permeability contrast ($k_2/k_1 = 0.9$) there was in general a low sensitivity to η_2/η_1. Since the system is close to the homogeneous case with $Ra = 200$ the convective effects dominate the system and consequently decreasing the thermal conductivity of the layer has little impact. The convective modes of this series were also characterized by 2D velocity distributions consisting of two convective cells. Stream lines of two examples are shown in Figure 11 and 3D temperature field in Figure 12, respectively.

4.3.2. Internal layer with high thermal conductivity ($\eta_2/\eta_1 > 1$)

On the other hand, the overall effect of increasing the thermal conductivity of the internal layer ($\eta_2/\eta_1 > 1$) was the attenuation of convection in the system. A constant decrease in Nu was observed in both permeability ratios that followed an approximately linear trend (Figure 8). Additionally, the correlation between Nu and η_2/η_1 displayed a weak dependence on the permeability ratio for the values analyzed. Two convective modes were observed in both permeability ratios, for $k_2/k_1 = 0.5$ the multiple cell convective mode shown in Figure 9

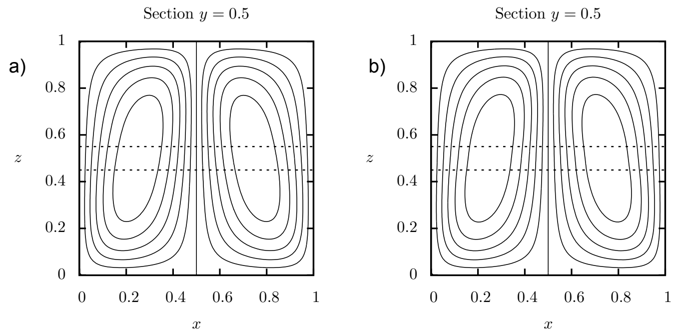

Figure 11: Stream lines for $k_2/k_1 = 0.9$ and a) $\eta_2/\eta_1 = 0.3$, b) $\eta_2/\eta_1 = 1.0$.

remains until $\eta_2/\eta_1 = 1.5$. Likewise, for $k_2/k_1 = 0.9$ the two cell regime remains until $\eta_2/\eta_1 = 1.8$, at these thermal diffusivity ratios the convection becomes single cell as shown in Figures 13 and 14.

5. Conclusion

Three-dimensional numerical simulations of free convection were carried out in a porous enclosure consisting of three layers of which the internal one was allowed to vary in permeability, thickness and thermal conductivity. The parametric study to evaluate the effect of decreasing the permeability of the internal

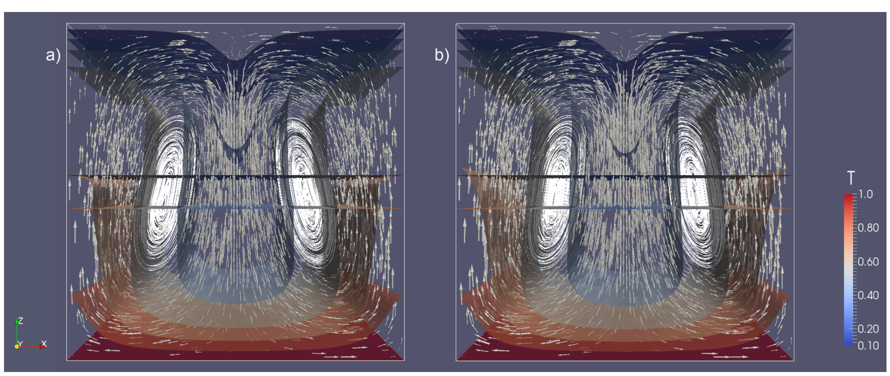

Figure 12: Steady-state solutions for $k_2/k_1 = 0.9$ and a) $\eta_2/\eta_1 = 0.3$, b) $\eta_2/\eta_1 = 1.0$.

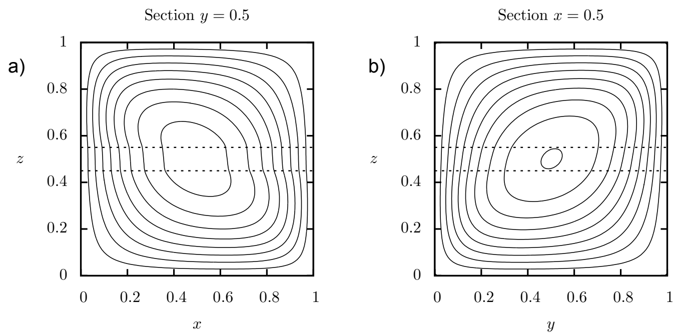

Figure 13: Stream lines for a) $k_2/k_1 = 0.5$ and $\eta_2/\eta_1 = 1.6$ and b) $k_2/k_1 = 0.9$ and $\eta_2/\eta_1 = 1.8$.

layer on the Nusselt number showed that permeability ratios lower than 0.6 are required to observe an appreciable drop in Nu. In agreement with this behaviour increasing the thickness of the middle layer had little impact on Nu in the range $0.6 \gtrsim k_2/k_1 < 1$. The steady-state convective modes attained in this parametric study were all characterized by two-dimensional velocity distributions. The three thicknesses analyzed displayed the same convective modes until $k_2/k_1 = 0.4$, in this range of permeability ratios the Nusselt number was, as expected, inversely proportional to h. For permeability ratios between 0.1

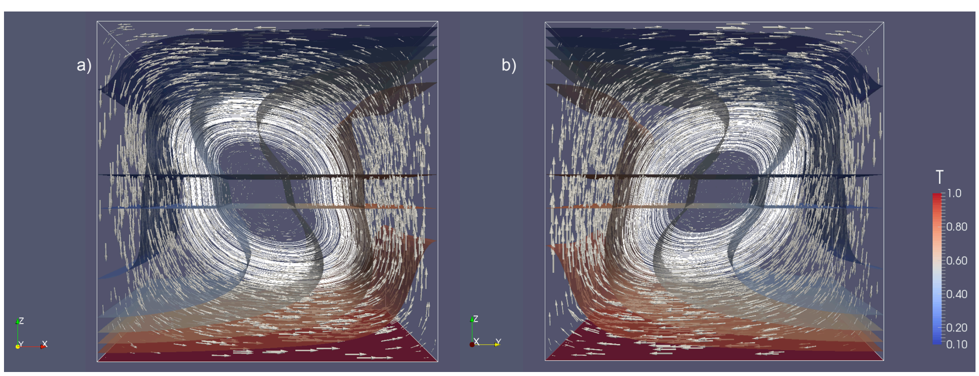

Figure 14: Steady-state solutions for a) $k_2/k_1 = 0.5$ and $\eta_2/\eta_1 = 1.6$ and b) $k_2/k_1 = 0.9$ and $\eta_2/\eta_1 = 1.8$.

and 0.3 the convective modes attained by $h = 0.1$ were different to those for $h = 0.15$ and $h = 0.2$. The thickness $h = 0.1$ developed four convective rolls partially of fully confined in the top and bottom layers, whereas $h = 0.15$ and $h = 0.2$ were characterized by a single cell with two secondary internal cells, this convective mode turned out to enhance the convective heat transfer of the porous enclosure and consequently the Nusselt number was higher in these cases than that for the thinest layer $h = 0.1$. The inverse proportionality relation of Nu with h was recovered at the highest permeability contrast $k_2/k_1 = 0.01$ for which the convection of $h = 0.1$ and $h = 0.15$ was confined convective rolls and $h = 0.2$ led to a conductive solution.

A slight enhancement of the heat transfer in the enclosure was produced when the thermal diffusivity of the middle layer was decreased up to moderate values. The porous enclosure with a weak permeability contrast $k_2/k_1 = 0.9$ presented a low sensitivity to the decrease, which indicates the dominance of convection in the system. Regarding the permeability ratio $k_2/k_1 = 0.5$, after the slight increase in Nu referred above, the system experienced a monotonic decrease in Nu as the thermal diffusivity of the middle layer was further decreased. At this permeability ratio the layer acted more effectively as a barrier for the heat flux. On the other hand, increasing the thermal diffusivity of the middle layer had a more consistent effect in the two permeability ratios analyzed, which was an approximately linear decrease in Nu. Two different convective modes were observed in this case: a dual-cell regime at moderate thermal diffusivity ratios and a single-cell regime at high ratios. However, the transition between these convective modes also appeared to be dependent on the permeability contrast.

This work has permitted us to qualitatively characterize important features of 3D convection in a layered porous medium. Extension of such an approach to real systems, such as geothermal reservoirs, would require definition of a parameter space reflecting robust models of the co-variance of thermal conductivity and permeability. No unique model of such co-variance exists however, as thermal conductivity is largely controlled by mineralogical composition, whereas permeability is principally controlled by independent physical phenomena. Case-specific parameterization would therefore be required in all instances for real natural domains.

Acknowledgement

This work was developed under the auspices of Consejo Nacional de Ciencia y Tecnología (CONACYT) and Cluff Geothermal Ltd.

References

[1] T. Graf, R. Therrien, Stable-unstable flow of geothermal fluids in fractured rock, Geofluids 9 (2009) 138–152.

[2] H. Gvirtzman, G. Garven, G. Gvirtzman, Thermal anomalies associated with forced and free ground-water convection in the dead sea rift valley, Geological Society of America Bulletin 109 (1997) 1167–1176.

[3] L. Guillou-Frottier, C. Carre, B. Bourgine, V. Bouchot, A. Genter, Structure of hydrothermal convection in the upper rhine graben as inferred from corrected temperature data and basin-scale numerical models, Journal of Volcanology and Geothermal Research 256 (2013) 29–49.

[4] A. Souche, M. Dabrowski, T. B. Andersen, Modeling thermal convection in supradetachment basins: example from western Norway, Geofluids 14 (2014) 58–74.

[5] R. McKibbin, M. J. O'Sullivan, Onset of convection in a layered porous-medium heated from below, Journal of Fluid Mechanics 96 (1980) 375–393.

[6] R. McKibbin, M. J. O'Sullivan, Heat-transfer in a layered porous-medium heated from below, Journal of Fluid Mechanics 111 (1981) 141–173.

[7] J. Richard, J. Gounot, Criterion for the onset of natural-convection in stratified porous layers, International Journal of Heat and Mass Transfer 24 (1981) 1325–1334.

[8] N. D. Rosenberg, F. J. Spera, Role of anisotropic and or layered permeability in hydrothermal convection, Geophysical Research Letters 17 (1990) 235–238.

[9] R. McKibbin, P. A. Tyvand, Anisotropic modeling of thermal-convection in multilayered porous-media, Journal of Fluid Mechanics 118 (1982) 315–339.

[10] J. Y. Jang, W. L. Tsai, Thermal-instability of 2 horizontal porous layers with a conductive partition, International Journal of Heat and Mass Transfer 31 (1988) 993–1003.

[11] D. A. S. Rees, G. Genç, The onset of convection in porous layers with multiple horizontal partitions, International Journal of Heat and Mass Transfer 54 (2011) 3081–3089.

[12] P. M. Patil, D. A. S. Rees, The onset of convection in a porous layer with multiple horizontal solid partitions, International Journal of Heat and Mass Transfer 68 (2014) 234–246.

[13] D. R. Hewitt, J. A. Neufeld, J. R. Lister, High Rayleigh number convection in a porous medium containing a thin low-permeability layer, Journal of Fluid Mechanics 756 (2014) 844–869.

[14] D. A. Nield, A. V. Kuznetsov, The effects of combined horizontal and vertical heterogeneity on the onset of convection in a porous medium, International Journal of Heat and Mass Transfer 50 (2007) 1909–1915.

[15] D. A. Nield, A. V. Kuznetsov, The effects of combined horizontal and vertical heterogeneity on the onset of convection in a porous medium: Moderate heterogeneity, International Journal of Heat and Mass Transfer 51 (2008) 2361–2367.

[16] F. Capone, M. Gentile, A. Hill, Convection problems in anisotropic porous media with nonhomogeneous porosity and thermal diffusivity, Acta Applicandae Mathematicae 122 (2012) 85–91.

[17] D. A. Nield, A. V. Kuznetsov, Onset of convection with internal heating in a weakly heterogeneous porous medium, Transport in Porous Media 98 (2013) 543–552.

[18] H. K. Versteeg, W. Malalasekera, An Introduction to Computational Fluid Dynamics, The Finite Volume Method, Prentice Hall, 1995.

[19] F. J. Guerrero-Martínez, P. L. Younger, K. Nader, Three-dimensional numerical modeling of free convection in sloping porous enclosures, International Journal of Heat and Mass Transfer 98 (2016) 257–267.

[20] J. Bear, Hydraulics of groundwater, McGraw-Hill, 1979.